IEEE Photonics Journal
An IEEE Photonics Society Publication

A Method to Reduce the Algorithm Complexity of the Single-Photodiode-per-Polarization Coherent Receiver

Volume 12, Number 1, February 2020

Keji Zhou
Sheng Cui
Yicong Tu
Deming Liu

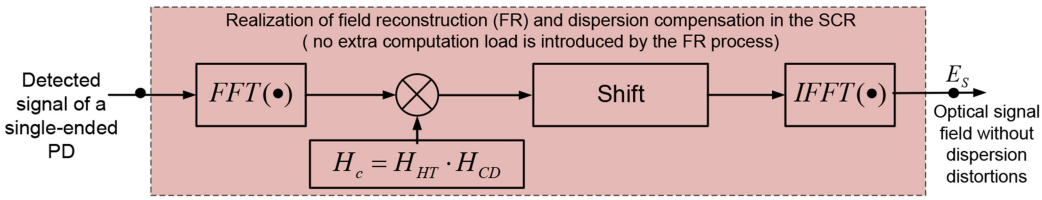

DOI: 10.1109/JPHOT.2019.2961108

A Method to Reduce the Algorithm Complexity of the Single-Photodiode-per-Polarization Coherent Receiver

Keji Zhou, Sheng Cui, Yicong Tu, and Deming Liu

[1]Wuhan National Laboratory for Optoelectronics, and School of Optical and Electronic Information, Huazhong University of Science and Technology, Wuhan 430074, China
[2]National Engineering Laboratory for Next Generation Internet Access System, Huazhong University of Science and Technology, Wuhan 430074, China

DOI:10.1109/JPHOT.2019.2961108

Manuscript received November 16, 2019; revised December 11, 2019; accepted December 17, 2019. Date of publication December 20, 2019; date of current version January 9, 2020. This work is supported by the National Natural Science Foundation of China (NSFC) under Grants 61975059 and 61975063.
Corresponding author: Sheng Cui (e-mail: cuisheng@hust.edu.cn).

Abstract: Single-photodiode-per-polarization coherent receivers (SCRs) can preserve all of the merits of the conventional digital coherent receivers (DCRs) such as supporting chromatic dispersion (CD) compensation and polarization multiplexing, whilst have much lower optical complexity. But the overall algorithm complexity of the SCRs is relatively higher because an extra dedicated field reconstruction algorithm (FRA) is required in addition to the standard algorithms used in DCRs. The heavy computation burden introduced by the FRA poses a major obstacle to reduce the DSP chip size and power consumption. In this paper we propose a method to reduce the overall algorithm complexity of the SCR by utilizing several techniques, including utilizing a strong local oscillator (LO) to mitigate the signal-signal beat interference (SSBI), a pseudo-single-side-band signal to recovery the signal field and a new FRA to reuse the operations in the CD compensation algorithm to realize field reconstruction. Other than reducing the overall algorithm complexity, the new method also make the SCR more robust to laser frequency offset compared with the existing heterodyne detection based FRA. Numerical simulations and experiments are presented to demonstrate the merits of new method with respect to the existing ones.

Index Terms: Chromatic dispersion compensation, computation complexity, field reconstruction algorithm, heterodyne detection, real-time DSP system, simplified coherent receivers.

1. Introduction

Conventional digital coherent receivers (DCRs) based on polarization and phase diversity techniques have a very high sensitivity and can support chromatic dispersion (CD) compensation and polarization multiplexed signals [1]–[6]. Owning to these merits DCRs are now widely used in high speed optical transmission systems. But conventional DCRs require two optical hybrids, four balanced-photodiodes and four analog to digital converters (ADCs), and thus are too expensive and power-consuming, especially for metropolitan, inter-data center and access optical networks. Recently various kinds of single-photodiode-per-polarization coherent receivers (SCRs) preserving all of the merits of the conventional DCRs have been proposed [7]–[17]. Such SCRs have much lower optical complexity and may potentially reduce the power consumption and ease the

monolithic integration. For this reason they have attracted much attention in the coherent optical communication field.

By the working principles the SCRs proposed by now can be mainly classified into two kinds. The first kind of SCRs necessitates an extra signal field reconstruction algorithm (FRA) to mitigate the signal-signal beat interference (SSBI) generated in the square-law detection to reconstruct the signal field [7]–[13]. Some of them treat SSBI as a perturbation and try to estimate and subtract it from the detected signal [7]–[10]. While the Kramers-Kronig (KK) receiver treats the detected signal as the intensity of a single-sideband minimum phase signal. Under this assumption the optical phase of the signal can be reconstructed by the Hilbert transform (HT) relation between the phase and natural logarithm of the detected signal [11]–[14]. The KK receiver provides superior performance compared with the other SSBI mitigation algorithms [11]. But a shortcoming of KK receivers is that due to the signal bandwidth increase resulting from the nonlinear square-root and logarithm operations, digital upsampling and a relatively higher oversampling rate of 4 samples per symbol (SPS) is often required, and thus the DSP system must operate at least two times as fast as that in conventional DCRs [11]–[14]. By now, several algorithms have been proposed to avoid digital upsampling in KK receivers [11], [13]. But they require one or two more HTs which are also computation expensive [18]–[20].

The second kind of SCRs utilizes optical domain schemes to mitigate SSBI [15], [16], [22]. Some of them add a frequency gap between the local oscillator (LO) and modulated signal spectrum to separate the linear LO-signal beat signal from the unwanted SSBI generated in the square-law detection [15], [16]. However the frequency gap results in a reduction of the spectral efficiency by at least a factor of 2. Recently a spectral efficient digital heterodyne detection (HD) based SCR (HD-SCR) is proposed [22]. Instead of adding a frequency gap, HD-SCR utilizes a strong LO to mitigate SSBI and thus doesn't need a dedicated FRA to deal with SSBI. But because HD requires a phase-locked loop (PLL) to recover the baseband signal, the HD-SCR still requires an extra dedicated FRA to realize the functions of the PLL [22]. Moreover the HD based FRA (HD-FRA) is not robust to the LFO as it has to compensate LFO at the very beginning of the DSP chain. At this point it is difficult to estimate LFO accurately.

For most high-speed optical communication systems CD compensation is mandatory in the coherent receiver. Frequency domain equalization outperforms time domain equalization with respect to implementation complexity over a wide range of CD values [23]. But with the existing SCRs such as the KK receiver and HD-SCR, CD compensation algorithm (CDCA) and other standard DSP algorithms (such as polarization demultiplexing and equalization) must be performed after the signal field is reconstructed with an extra dedicated FRA. Thus the overall algorithm complexity of the existing SCRs is relatively higher compared with the conventional DCRs. The extra heavy computation burden introduced by the FRA poses a major obstacle to realize high speed real-time SCRs and reduce the DSP chip size and power consumption. Thus reducing the overall algorithm complexity of SCRs is imperative for practical applications.

In this paper we propose a method which can greatly reduce the algorithm complexity of the SCR whilst preserves the benefits of the DCRs, including exceptionally high sensitivity, robustness to chromatic dispersion and LFO. To achieve this goal, we utilize several techniques in combination, including a strong LO to mitigate the SSBI, a pseudo-single-side-band (PSSB) signal to recovery the signal field and a new FRA to reuse the operations in CDCA for field reconstruction. Moreover the new FRA is also more robust to LFO compared with the existing HD-FRA. This paper is organized as follows. Section 2 describes the working principles of the new method and compares it with the existing ones. Section 3 provides numerical simulation and experimental results to demonstrate the merits of the SCR designed with the proposed method with respect to other SCRs. Finally conclusions are drawn in Section 4.

2. Working Principles

Fig. 1 shows the setup of the polarization diversity SCRs such as the polarization diversity KK receiver and HD-SCR [22], [24]. In each polarization the optical signal is combined with the LO

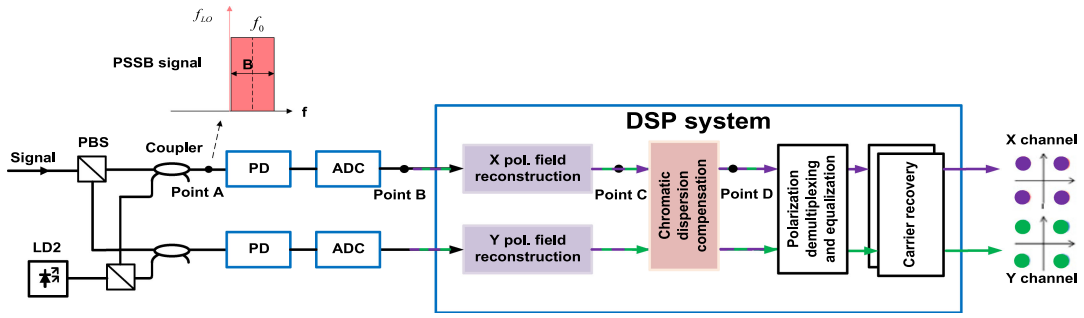

Fig. 1. The setup of the polarization-diversity SCR and its DSP system. PBS stands for polarization beam splitter.

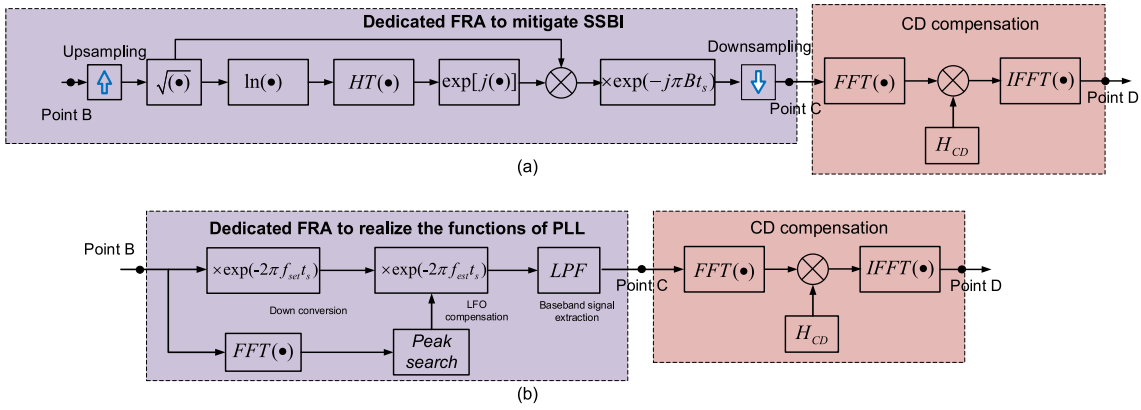

Fig. 2. The detailed flow charts of the DSP algorithms between the points B and D in Fig. 1 for the KK receiver (a) and HD-SCR (b). The operations highlighted by the purple rectangles can be removed by our method.

and then detected by a single-ended photodiode. The output signal is digitalized by the ADC and then input into the DSP system for field reconstruction. Once the X and Y polarization fields are recovered using the FRA respectively, the following DSP algorithms, including CD compensation, polarization de-multiplexing and equalization and carrier recovery can use the standard DSP algorithms in the conventional DCRs [22], [24]. Fig. 2 shows the detailed flow charts of the DSP algorithms between points B and D in Fig. 1 for the KK receiver and HD-SCR, respectively. As can be seen here, KK receiver requires a dedicated FRA to mitigate the SSBI [11], while the HD-SCR utilizes a strong LO to mitigate the SSBI. But the HD-SCR still relies on a dedicated FRA to realize the functions of PLL [22]. CD compensation is realized with the standard frequency domain CDCA consisting of one forward fast Fourier transform (FFT) followed by frequency domain multiplication with the inverse CD transfer function and one final inverse FFT (IFFT) [23]. As can be seen on Fig. 1 and Fig. 2, the overall algorithm complexity of SCR is higher compared with the conventional DCRs due to the extra FRA stage.

With our method the algorithm complexity of the SCR can be greatly reduced and all of the operations highlighted by the purple rectangles in Fig. 2 can be removed. Fig. 3(a) shows the detailed flow charts of the DSP algorithms between points B and D in Fig. 1 for the SCR designed by our method. As can be seen here, an extra FRA stage is not required any more. It is merged with the CDCA stage. To illustrate the working principles of our method, Fig. 3(b) plots the flow charts of the new FRA and CDCA separately. For one polarization component, the input signal and

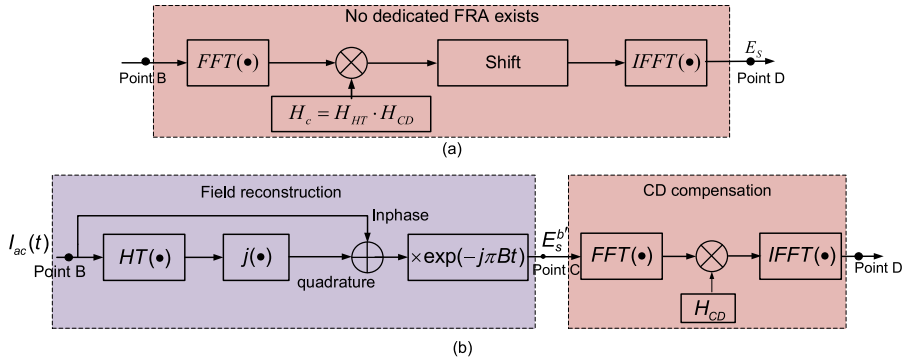

Fig. 3. The detailed flow charts of the DSP algorithms between the points B and D in Fig. 1 when our method is adopted.

LO can be written as follows

$$\begin{aligned} E_S(t) &= A_S(t)\exp\{j[\omega_s t + \phi_S(t)]\} \\ &= \{A_S(t)\cos[\phi_S(t)] + jA_S(t)\sin[\phi_S(t)]\}\exp(j\omega_s t) \\ &= [I(t) + jQ(t)]\exp(j\omega_s t) \\ &= E_s^b \exp(j\omega_s t), \end{aligned} \tag{1}$$

$$E_{LO}(t) = A_{LO}\exp\{j[\omega_{LO} t + \phi_{LO}(t)]\}. \tag{2}$$

Here $A_S(t)$ and A_{LO} stand for the amplitudes of the signal and LO field. $\omega_{s,LO}$ stand for the center angular frequencies of the input optical signal and LO, respectively. $\phi_{S,LO}(t)$ stand for the signal and LO phases, respectively. $I(t)$ and $Q(t)$ stand for the real and imaginary parts of the baseband complex signal $E_s^b = I(t) + jQ(t)$, respectively. Noise is not considered here for simplicity and clarity. When the offset between the continuous wave (CW) LO and the modulated signal is half of the input signal optical bandwidth B, the two can constitute an optical single-side-band (SSB) signal because the same optical signal can also be generated by modulating the CW LO (acting as a CW carrier) with a SSB signal [16] having the following form

$$E_{SSB}(t) = E_s^b \exp[j(\omega_s - \omega_{LO})t] = E_s^b \exp(j\pi Bt) = I_{SSB}(t) + j \cdot Q_{SSB}(t). \tag{3}$$

Without loss of generality, here we assume that $(\omega_s - \omega_{LO})/2\pi = (f_s - f_{LO}) = B/2$. In other words, the SSB signal $E_{SSB}(t)$ is obtained by shifting the baseband signal E_s^b within [−B/2, B/2] to the positive frequency band of [0, B] so that the negative frequencies of $E_{SSB}(t)$ are zero. $I_{SSB}(t)$ and $Q_{SSB}(t)$ stand for the real and imaginary parts of the SSB signal, respectively, and -The latter is the HT of the former [16]. Thus, if $I_{SSB}(t)$ can be obtained somehow, the imaginary part $Q_{SSB}(t)$ can be obtained by taking a HT of $I_{SSB}(t)$. Then the complex SSB signal field $E_{SSB}(t)$ can also be obtained. Subsequently the baseband signal field E_s^b can be recovered by simply multiplying $E_{SSB}(t)$ with $\exp(-j\pi Bt)$. But in practice the LO acting as the carrier and the modulated signal are generated from two different lasers located at the receiver and transmitter, respectively. Considering the inevitable LFO and laser phase noise (LPN) of the LO, the SSB signal actually has the following form

$$E'_{SSB}(t) = E_s^b \exp\{j[(\pi B + \Delta\omega_{LFO})t - \phi_{LO}]\} = E_s^{b\prime} \exp(j\pi Bt), \tag{4}$$

where $\Delta\omega_{LFO}$ and ϕ_{LO} stand for the LFO and LPN, respectively. We refer to $E'_{SSB}(t)$ as a pseudo-single-side-band (PSSB) signal as it not only contains the information modulated on the optical carrier but also LFO and LPN of the LO. The baseband signal can still be obtained from the PSSB signal by multiplying $E'_{SSB}(t)$ with $\exp(-j\pi Bt)$ but now it has the following form

$$E_s^{b\prime} = E_s^b \exp[j(\Delta\omega_{LFO} t - \phi_{LO})]. \tag{5}$$

Thus the baseband signal obtained is also affected by LFO and LPN. Nevertheless after E_s^{br} is obtained, the LFO and LPN effect can be easily mitigated by the standard robust digital carrier recovery algorithm. So the remaining problem is how to obtain the real part of the PSSB signal which has the following form

$$I'_{SSB}(t) = \mathrm{Re}[E'_{SSB}(t)] = A_S(t)\cos[(\pi B + \Delta\omega_{LFO})t + \phi_S(t) - \phi_{LO}(t)]. \tag{6}$$

As shown in Fig. 1 the detected signal $I_p(t)$ output by the single-ended photodiode has the following form

$$I_p(t) = R\left|E_S(t) + E_{LO}(t)\right|^2 = RA_{LO}^2 + R\left|A_S(t)\right|^2 + 2RA_{LO}A_S(t)\cos[(\omega_s - \omega_{LO})t + \phi_S(t) - \phi_{LO}(t)]. \tag{7}$$

Here R represents the photodiode responsitivity. The three items on the right side of Eq. (7) represent the DC current related to the LO power, the unwanted SSBI current and the linear LO-signal beat current, respectively. The DC current can be eliminated by AC coupling. The SSBI current $I_{SSBI}(t) = R|A_S(t)|^2$ can be suppressed by adding a strong LO to amplify the LO-signal beat current only. By this simple SSBI mitigate technique $I_p(t)$ is approximately equal to

$$I'_p(t) = 2RA_{LO}A_S(t)\cos[(\omega_s - \omega_{LO})t + \phi_S(t) - \phi_{LO}(t)] = 2RA_{LO}I'_{SSB}(t). \tag{8}$$

When LFO is considered, $\omega_s - \omega_{LO} = \pi B + \Delta\omega_{LFO}$. Thus $I'_p(t)$ and $I'_{SSB}(t)$ are actually the same except the constant factor $2RA_{LO}$. In summary by utilizing a strong LO to suppress SSBI and the PSSB signal to recover the imaginary part, field reconstruction can be realized using a single-ended photodiode. But as shown in Fig. 3(b) an extra FRA consisting of one HT, one complex multiplication and one addition is still required for the time being.

To reduce the computation effort and benefit from the already existing FFT/IFFT and multiplication operations in CDCA, HT in the new FRA is performed in the frequency domain by the following method. First N-point FFT of the samples of $I'_p(t)$ is computed by FFT. The obtained Fourier transform block V is element-wisely multiplied with a frequency domain transfer function H_{HT} given by

$$H_{HT} = \begin{cases} 1 & 1, N/2+1 \\ 2 & 2, 3, \ldots, N/2 \\ 0 & N/2+2, \ldots, N \end{cases}. \tag{9}$$

After taking an inverse FFT (IFFT), the PSSB signal field $E'_{SSB}(t)$ whose imaginary part is the HT of the real part can be obtained taking advantage of the property of the analytical signal [20]. The interested reader is referred to Ref. [21] for further details of the HT algorithm. The above FFT/IFFT and multiplication operations are exactly the same as those in the CDCA. As shown in Fig. 3(a), the FRA and CDCA can be performed simultaneously by sharing these operations and using a combined transfer function given by

$$H_c = H_{CD} \cdot H_{HT}, \tag{10}$$

where

$$H_{CD}(f) = \exp\left[-j\frac{\pi c \cdot D_t \cdot (f - B/2)^2}{f_s^2}\right]. \tag{11}$$

Here D_t is the accumulated fiber dispersion. It is noteworthy that V is actually the Fourier transform of the PSSB signal $E'_{SSB}(t)$. So the frequency shifting operation $\times \exp(-j\pi Bt)$ in Fig. 3(b) can be replaced by shifting the elements in V as shown in Fig. 3(a). Finally after taking an IFFT, the baseband complex signal E_s^{br} can be obtained. It is noteworthy that H_{HT} consists of only 1, 2 and 0, so the calculation of H_c doesn't require any multiplication ($\times 2$ can be implemented simply by using a 1-bit shift, instead of using a multiplier).

In summary, utilizing a strong LO to suppress SSBI, a PSSB signal to recover the signal field, and a new FRA to reuse the operations in CDCA to realize field reconstruction, the overall algorithm complexity of the SCR can be greatly reduced. Comparing the new DSP chain shown in Fig. 3(a)

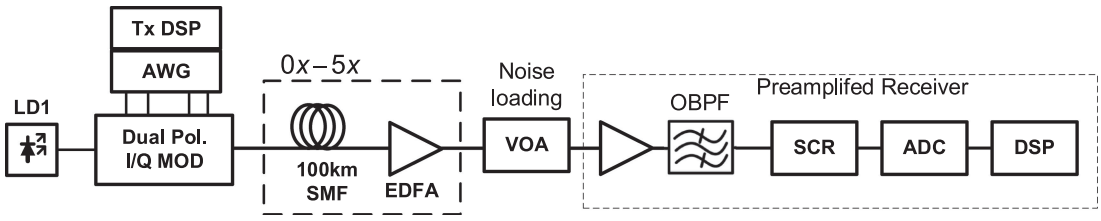

Fig. 4. The setup of the transmission system used to investigate the performance of the SCRs.

with the standard one used in DCRs [1], we find the two have nearly the same algorithm complexity. But DCRs have a much higher optical complexity and suffer from the front-end distortions incurred by non-ideal optical hybrids and balanced-photodiodes, while the SCR hasn't such a problem. The lower optical complexity and front-end distortions are a unique advantage over the traditional DCRs.

Compared with existing SCR such as the KK receiver and HD-SCR, the new SCR has a much lower DSP complexity. All of the extra operations required by the KK receiver and HD-SCR highlighted with the purple rectangles in Fig. 2 can be removed by our method. Comparing the new DSP chain shown in Fig. 3(a) with the KK scheme shown in Fig. 2(a), we can find that the former removes the operations like digital upsampling, square root, logarithm and one HT. Thus the requirement on the DSP chip size and processing speed can be greatly reduced. Although the carrier (LO) to signal power ratio (CSPR) required by the new method is higher, it can be readily satisfied as the LO is inside the receiver and its power is generally much higher than the input optical signal which has experienced a large transmission loss.

Compared with the HD-SCR, other than reducing the overall algorithm complexity the new SCR is also more robust to LFO. In the HD-FRA a digital low pass filter (LPF) must be used to extract the down-converted signal out as shown in Fig. 2(b). But in practice the down-converted signal is not at baseband due to LFO. So the HD-FRA has to compensate LFO first. At this point of DSP chain it is difficult to estimate LFO accurately as the signal field is not reconstructed yet. Although LFO can be estimated by searching the signal spectrum peak in the frequency domain [22], but an extra FFT is required and the estimation error may be large when the signal spectrum has a flat top (such as the Nyquist signals with a small roll-off factor) or is distorted by the cascaded optical nodes containing non-ideal optical filtering elements [25], [26]. Compared with the HD-FRA, the new FRA has the following advantages: 1) LFO hasn't to be compensated at the very beginning of the DSP chain. It can be compensated later by the standard carrier recovery algorithm which is more robust to LFO. 2) The extra FFT, two complex multiplications, peak search and LPF operations are not required so the requirement on the DSP chip size can be reduced.

3. Numerical Simulations and Experiments

We investigate the performance of the SCRs in the 10 GBaud polarization-multiplexed Nyquist QPSK transmission system shown in Fig. 4 by both numerical simulations and experiments. In the numerical simulation the commercial software VPI TransmissionMaker is used. In the experiment we use an arbitrary waveform generator (AWG) with an electrical 3-dB bandwidth of 25 GHz and a sampling rate of 40 GSa/s to generate the analog signals corresponding to the in-phase and quadrature components of the Nyquist-pulse-shaped QPSK signal. These signals are amplified with a linear driver amplifier and connected to a high-bandwidth I/Q modulator which is fed by an external cavity laser (ECL) at 1550 nm. The power of the LO of the SCR is fixed at -1 dBm as the maximal input power of the photodiode we used is limited to 0 dBm. A variable optical attenuator (VOA) in front of the receiver is used to control the input signal power and set the carrier (LO) to signal power ratio (CSPR). A 3-dB optical coupler is used to combine the input signal with the LO whose frequency is shifted by 5.1 GHz with respect to the first ECL. The small frequency gap

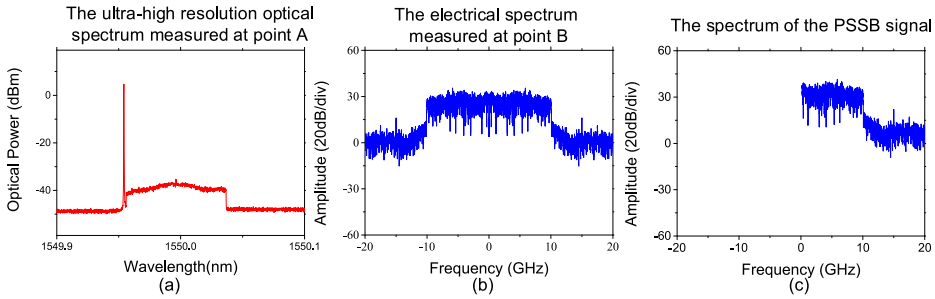

Fig. 5. The experimental optical spectrum measured at point A (a). The experimental digitalized spectra of the signal at point B (b) and of the PSSB signal (c).

of 100 MHz ensures that the SSB signal condition can be satisfied when LFO is present. Single-ended photodiodes with 40 GHz bandwidth are used to detect the optical signal. The detected AC electrical signals are sampled by a real-time oscilloscope (RTO) with an electrical 3-dB bandwidth of 36 GHz and sampling rate of 80 GSa/s. The sampled signals are stored and processed off-line by a computer. As regard to the off-line processing, the signal is first down-sampled to satisfy the Nyquist sampling rate only which is 2 times the bandwidth of $I'_p(t)$ and then the new algorithm shown in Fig. 3(a) is used to recover the signal field and compensate CD. Subsequently the standard algorithms including the constant module algorithm (CMA), differential M-th power LFO estimation algorithm and Viterbi-Viterbi algorithm are used to realize polarization demultiplexing, LFO and LPN compensation [1], [2]. To characterize the new SCR performance, we either perform ASE noise loading in a back-to-back configuration or transmit the signal over up to 5 spans of 100 km standard single-mode fiber (SSMF) having a dispersion coefficient of 16 ps/nm/km and loss of 0.2 dB/km.

Fig. 5(a) shows the experimental optical spectrum at point A in Fig. 1 which is measured with an ultra-high resolution Brillouin optical spectrum analyzer (BOSA) [27]. As we can see, the spectrum consists of the LO (the strong narrow spectral line) and Nyquist QPSK signal with a rectangular-like spectrum whose center peak is very weak. Fig. 5(b) shows the experimental electrical spectrum of the signal output by the photodiode. As we can see, it is a double side band (DSB) signal with a bandwidth of about 20 GHz. Fig. 5(c) shows the spectrum of the PSSB signal obtained by the new FRA in the field reconstruction process. As we can see, it is a SSB signal with a bandwidth of about 10 GHz. The baseband complex signal can be obtained by shifting it to the left in the frequency domain.

In the real-time DSP platform the frequency domain HT consisting of FFT and IFFT operations must be implemented in a blockwise manner. Thus the edge effect incurring distortions in the beginning and in the end of the processed block must be considered [11]. To mitigate the edge effect we utilize the overlapped and save technique [23]. The overlapped parts on both edges of the processed block with a length of N_d are discarded. Fig. 6(a) shows the variations of error vector magnitude (EVM) versus the received signal OSNR for different N_d obtained by numerical simulations in the back-to-back system. Here the FFT block size (N) is set to be equal to 256. As we can see, the performance obtained with $N_d = 32$ is much better than that obtained with $N_d = 0$ and is close to that obtained with $N_d = 96$. Considering the balance between the efficiency and performance, (N, N_d) of (256, 32) is adopted in the following investigation. When fiber dispersion is present the required N_d for a transmission distance of 500 km is 13 according to the analysis in [23]. Thus $N_d = 32$ is also sufficient for mitigating the inter-block interference (IBI) due to CD.

Fig. 6(b) shows the variations of BER as a function of the received signal OSNR for the back-to-back and 500 km transmission system, respectively. The data points stand for the experimental results while the solid and dashed lines represent the simulation results. The dash-dotted line represents the theoretical limit. The magnitude and phase frequency responses of H_c used for L = 0 and 500 km are shown in Fig. 7(a). As we can see, the back-to-back experiment shows that

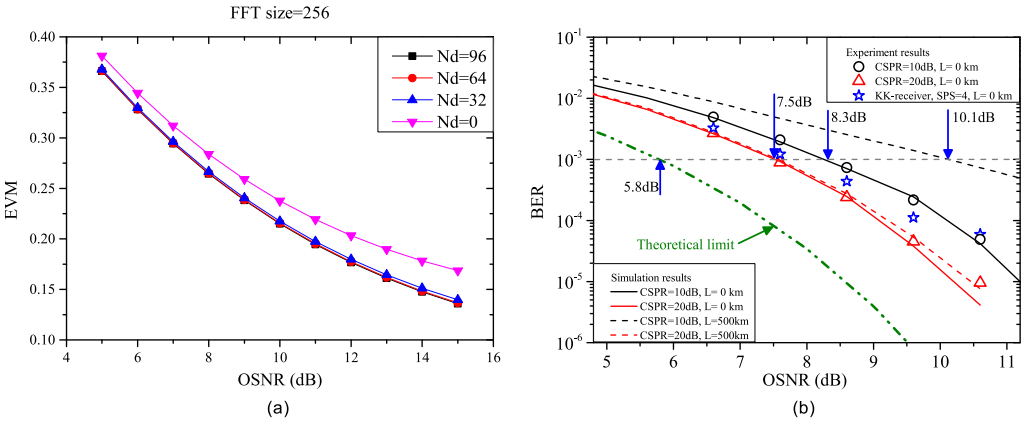

Fig. 6. (a) The variations of error vector magnitude (EVM) versus the received signal OSNR for different N_d obtained by numerical simulations in the back-to-back system. (b) The variations of BER versus the received signal OSNR obtained by numerical simulations and experiments for the back-to-back and L = 500 km transmission system.

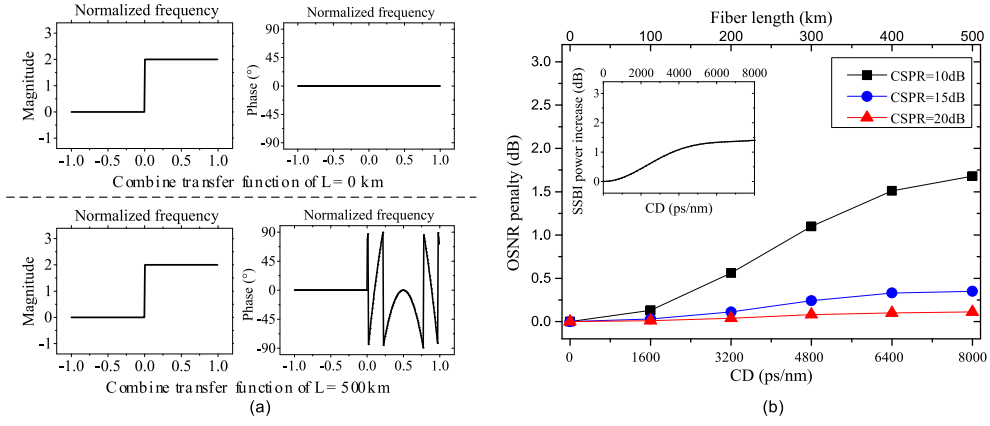

Fig. 7. (a) The magnitude and phase frequency responses of H_c. (b) The variations of the OSNR penalty versus the accumulated CD for different CSPR. The inset shows the variation of the SSBI power versus the accumulated CD.

the OSNR penalty from the theoretical limit (@BER = 10^{-3}) is 2.5 dB when CSPR is set to be 10 dB in the new SCR because the SSBI is not adequately suppressed. But when CSPR is set to be 20 dB, OSNR penalty from the theoretical limit can be reduced to 1.7 dB, which is close to that of the full-fledged DCRs. The experimental results of the KK receiver are also given in Fig. 6(b). For the KK receiver digital upsampling is performed to raise from the Nyquist sampling rate to SPS = 4. In this condition the KK receiver can achieve a similar sensitivity as the new SCR but its requirement on the DSP chip is much higher as mentioned above. When the signal is transmitted up to 500 km, the OSNR penalty increases to 4.3 dB when CSPR = 10 dB as the SSBI power increases with CD. But the OSNR penalty keeps the nearly same when CSPR = 20 dB. It proves that the new SCR with an adequate CSPR is robust to the accumulated CD. Fig. 7(b) shows the variations of the OSNR penalty versus the accumulated CD for different CSPR. The inset shows the variations of the SSBI power $P_{SSBI} = < I^2_{SSBI}(t) >$ versus the accumulated CD. As we can see, the SSBI power increases by about 1.5 dB when CD is increased from 0 to 8000 ps/nm. For the new SCR, the OSNR penalty increases by about 1.8 and 0.3 dB when CSPR = 10 and 15 dB, respectively. But when CSPR = 20 dB the OSNR penalty increases by only 0.1 dB. A similar high sensitivity as the full-fledged DCRs can still be obtained as in the back-to-back system.

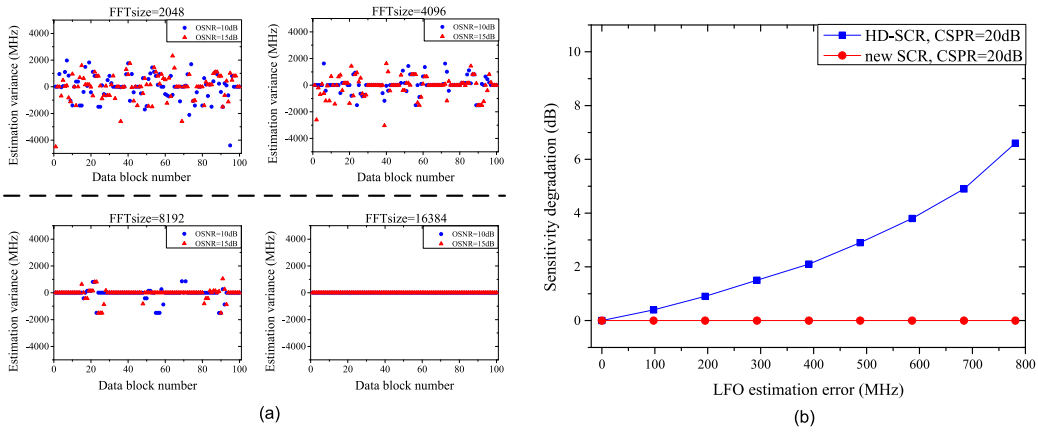

Fig. 8. (a) The LFO estimation error for different sample blocks. (b) The sensitivity degradation due to the LFO estimation error.

As mentioned above the HD-FRA is not suitable for the Nyquist signals with a flat-top spectrum. For example, Fig. 8(a) shows the LFO estimation variance obtained using the data blocks acquired in the back-to-back experiments for the Nyquist QPSK signal with OSNR = 10 and 15 dB. The FFT size used to calculate the down-converted signal spectrum is 2048, 4096, 8192 and 16384, respectively. In each figure 100 times of independent LFO estimations are carried out. The variance is defined by the deviation from the averaged value obtained with a FFT size of 16384 which is very stable and close to the real LFO value. The data blocks are acquired within 20 ms. Within such a short time the laser frequency drift is neglectable in the relatively stable laboratory environment, and thus the variance should be close to zero. But, as we can see, the variance is larger than 800 MHz until the FFT size is 16384. This is because the weak center peak of the Nyquist signal spectrum (as shown in Fig. 5(a)) is hard to identify until a very large FFT size is adopted to obtain a sufficiently high spectra resolution. Fig. 8(b) shows the variations of the OSNR penalty as a function of the LFO estimation error for the HD-SCR obtained by numerical simulations. In this figure the sampling rate is set to be equal to 2 times the down-converted signal bandwidth. As we can see, the OSNR penalty is about 7 dB when the LFO estimation error is 800 MHz. On the contrast the new SCR designed by our method is more robust to LFO because LFO can be compensated after the optical signal field reconstruction, chromatic dispersion compensation and polarization demultiplexing/equalization are performed, and thus the more robust and easier to implement standard blind differential M-th power LFO estimation algorithm can be applied. It is noteworthy that the training-based LFO estimation algorithms [28], [29] with lower complexity which is not suitable for the HD-SCR are also applicable in the new SCR and can reduce the complexity further at the cost of the overhead for the training symbols.

4. Conclusion

In this paper we propose a method to reduce the algorithm complexity of the SCR and eliminate the extra FRA stage required by the exiting SCRs. This method utilizes several techniques in combination to achieve this goal, including utilizing a strong LO to mitigate SSBI, a pseudo-single-side-band signal to recovery the signal field and a new FRA to reuse the operations in the CDCA to realize field reconstruction. Moreover the SCR designed by this method can preserve the all the merits of the DCRs, including exceptionally high sensitivity, robustness to chromatic dispersion and LFO, supporting polarization demultiplexing and advanced modulation formats. The competing requirements of reducing optical complexity and DSP algorithm complexity can be satisfied simultaneously for the first time by this method which is appealing for many high speed transmission systems with strict limitations on the cost and power consumption.

References

[1] S. J. Savory, "Digital coherent optical receivers: Algorithms and subsystems," *IEEE J. Sel. Topics Quantum Electron.*, vol. 16, no. 5, pp. 1164–1179, Sep./Oct. 2010.
[2] S. Bigo, "Coherent optical long-haul system design," in *Proc. Opt. Fiber Commun. Conf.*, 2012, Art. no. OTh3A.1.
[3] I. P. Kaminow, T. Li, and A. E. Willner, *Optical Fiber Telecommunications V* (Volume B Systems and Networks). Amsterdam, The Netherlands: Elsevier, 2008, ch. 2.
[4] X. Zhou, "Efficient clock and carrier recovery algorithms for single-carrier coherent optical systems: A systematic review on challenges and recent progress," *IEEE Signal Process. Mag.*, vol. 31, no. 2, pp. 35–45, Mar. 2014.
[5] L. G. Kazovsky, G. Kalogerakis, and W. Shaw, "Homodyne phase-shift-keying systems: Past challenges and future opportunities," *J. Lightw. Technol.*, vol. 24, no. 12, pp. 4876–4884, Dec. 2006.
[6] L. Gagnon, D. Sebastien, S. Tsukamoto, K. Katoh, and K. Kikuchi, "Coherent detection of optical quadrature phaseshift keying signals with carrier phase estimation," *J. Lightw. Technol.*, vol. 24, no. 1, pp. 12–21, Jan. 2006.
[7] K. Zou, Y. Zhu, F. Zhang, and Z. Chen, "Spectrally efficient terabit optical transmission with Nyquist 64-QAM half-cycle subcarrier modulation and direct-detection," *Opt. Lett.*, vol. 41, no. 12, pp. 2767–2770, 2016.
[8] S. Randel, D. Pilori, S. Chandrasekhar, G. Raybon, and P. Winzer, "100-Gb/s discrete-multi-tone transmission over 80-km SSMF using single-sideband modulation with novel interference-cancellation scheme," in *Proc. Eur. Conf. Opt. Commun.*, 2015, Art. no. Mo.4.5.2.
[9] Z. Li, M. S. Erkilinc, R. Maher, L. Galdino, K. Shi, and B. C. Thomsen, "Two-stage linearization filter for direct-detection subcarrier modulation," *IEEE Photon. Technol. Lett.*, vol. 28, no. 24, pp. 2838–2841, Dec. 2016.
[10] M. S. Erkilinc, Z. Li, R. Maher, L. Galdino, K. Shi, and B. C. Thomsen, "Reach enhancement for WDM direct-detection subcarrier modulation using low-complexity two-stage signal-signal beat interference cancellation," in *Proc. Eur. Conf. Opt. Commun.*, 2016, Art. no. M.2.B.1.
[11] A. Mecozzi, C. Antonelli, and M. Shtaif, "Kramers-Kronig coherent receiver," *Optica*, vol. 3, no. 11, pp. 1220–1227, 2016.
[12] Z. Li *et al.*, "SSBI mitigation and the Kramers–Kronig scheme in single-sideband direct-detection transmission with receiver-based electronic dispersion compensation," *J. Lightw. Technol.*, vol. 35, no. 10, pp. 1887–1893, May 2017.
[13] T. Bo and H. Kim, "Kramers-Kronig receiver operable without digital upsampling," *Opt. Exp.*, vol. 26, no. 11, pp. 13810–13818, 2018.
[14] Z. Li *et al.*, "Joint optimization of resampling rate and carrier-to-signal power ratio in direct-detection Kramers-Kronig receivers," in *Proc. Eur. Conf. Opt. Commun.*, 2017, Art. no. W.2.D.3.
[15] A. J. Lowery and J. Armstrong, "Orthogonal-frequency-division multiplexing for dispersion compensation of long-haul optical systems," *Opt. Exp.*, vol. 14, pp. 2079–2084, 2006.
[16] B. J. C. Schmidt, A. J. Lowery, and J. Armstrong, "Experimental demonstrations of electronic dispersion compensation for long-haul transmission using direct-detection optical OFDM," *J. Lightw. Technol.*, vol. 26, no. 1, pp. 196–203, Jan. 2008.
[17] J. Zhang *et al.*, "Simplified coherent receiver with heterodyne detection of eight-channel 50 Gb/s PDM-QPSK WDM signal after 1040 km SMF-28 transmission," *Opt. Lett.*, vol. 37, no. 19, pp. 4050–4052, 2012.
[18] T. Bo, R. Deng, J. He, and H. Kim, "On the hardware complexity of Kramers-Kronig receiver," in *Proc. IEEE Conf. Lasers Electro-Opt. Pacific Rim*, 2018, Art. no. Tu2I.2.
[19] A. Prince, P. K. Verma, C. Jayakumar, and D. Raju, "Efficient architecture for real time implementation of Hilbert transform in FPGA," in *Proc. IEEE Int. Conf. Elect., Comput., Commun. Technol.*, 2015, pp. 1–5.
[20] MathWorks, "Discrete-time analytic signal using Hilbert transform." 2019. [Online]. Available: https://www.mathworks.com/help/signal/ref/hilbert.html
[21] L. Marple, "Computing the discrete-time "analytic" signal via FFT," *IEEE Trans. Signal Process.*, vol. 47, no. 9, pp. 2600–2603, Sep. 2002.
[22] B. Corcoran, B. Foo, and A. J. Lowery, "Single-photodiode per polarization receiver with signal-signal beat interference suppression through heterodyne detection," *Opt. Exp.*, vol. 26, no. 3, pp. 3075–3086, 2018.
[23] R. Kudo, T. Kobayashi, K. Ishihara, Y. Takatori, A. Sano, and Y. Miyamoto, "Coherent optical single carrier transmission using overlap frequency domain equalization for long-haul optical systems," *J. Lightw. Technol.*, vol. 27, no. 16, pp. 3721–3728, Aug. 2009.
[24] X. Chen *et al.*, "4 $\times$ 240 Gb/s dense WDM and PDM Kramers-Kronig detection with 125-km SSMF transmission," in *Proc. Eur. Conf. Opt. Commun.*, 2017, Art. no. W.2.D.4.
[25] T. Rahman *et al.*, "On the mitigation of optical filtering penalties originating from ROADM cascade," *IEEE Photon. Technol. Lett.*, vol. 26, no. 2, pp. 154–157, Jan. 2014.
[26] H. Lu, S. Cui, C. Ke, and D. Liu, "Automatic reference optical spectrum retrieval method for ultra-high resolution optical spectrum distortion analysis utilizing integrated machine learning techniques," *Opt. Exp.*, vol. 25, no. 26, pp. 32491–32503, 2017.
[27] C. Xing, C. Ke, K. Zhang, Z. Guo, Y. Zhong, and D. Liu, "Polarization- and wavelength-independent SBS-based filters for high resolution optical spectrum measurement," *Opt. Exp.*, vol. 25, no. 18, pp. 20969–20982, 2017.
[28] S. Zhang, O. Omomukuyo, O. A. Dobre, X. Lin, and D. Chang, "Training-aided joint frame and frequency synchronization for THP FTN coherent optical systems," in *Proc. IEEE 20th Int. Conf. Transparent Opt. Netw.*, 2018, Art. no. Mo.C1.4.
[29] X. Zhou, X. Chen, and K. Long, "Wide-range frequency offset estimation algorithm for optical coherent systems using training sequence," *IEEE Photon. Technol. Lett.*, vol. 24, no. 1, pp. 82–84, Jan. 2012.